

Short Communication

Preparation of Ni-Co-Fe Alloy Coating on Copper by Ultrasound-assisted Electrodeposition and Its Mechanical Property

Juan Guo*, Xingling Yao

Xinxiang Vocational and Technical College, Xinxiang 453000, China

*E-mail: guo_teacher1612@126.com

Received: 13 March 2022 / *Accepted:* 26 April 2022 / *Published:* 6 June 2022

Ni-Co-Fe alloy coating was prepared on the surface of copper by ultrasound-assisted electrodeposition to improve the mechanical property of copper. The experimental results show that the special effects of ultrasound affect the mass transfer and nucleation during electrodeposition, which leads to differences in the mechanical property of Ni-Co-Fe alloy coatings. With the increase of ultrasound power, the grains of Ni-Co-Fe alloy coatings are refined and the microstructure tend to be compact resulting in the increase of hardness and elastic modulus which attributes to the enhancement of elastic recovery ability and wear resistance. However, too much higher ultrasound power leads to the deterioration of microstructure and decrease of hardness resulting in the decrease of elastic recovery and wear resistance of Ni-Co-Fe alloy coatings. The Ni-Co-Fe alloy coating electrodeposited under ultrasound power 120 W has nanocrystalline structure with average grain size of 50 nm and maximum hardness of 652.6 HV. Moreover, the elastic modulus reaches 202.4 GPa and the friction factor and wear amount are only 0.32 and 0.82 mg respectively. Compared with copper, the Ni-Co-Fe alloy coating electrodeposited under ultrasound power 120 W has good toughness, optimal elastic recovery and better wear resistance which can significantly improve the mechanical property of copper.

Keywords: Ni-Co-Fe alloy coating; ultrasound-assisted electrodeposition; mechanical property; ultrasound power

1. INTRODUCTION

Copper has excellent electrical conductivity, good thermal conductivity and nice ductility, but its mechanical property is poor, such as low hardness, small elastic modulus and poor wear resistance. Many works have shown that the chemical and physical properties of copper can be improved by surface strengthening treatment, so as to better meet the requirements of applications. At present, the technologies suitable for the surface strengthening treatment of copper mainly include

electrodeposition, chemical vapor deposition, thermal spraying, plasma bombardment and laser cladding [1-7]. Among them, electrodeposition has the advantages of simple process, low cost and high efficiency which is superior to other surface strengthening technologies.

Many researchers have used electrodeposition to strengthen the surface of copper to further improve the overall properties of the coating by optimizing the electrodeposition process conditions [8-12]. The results show that ultrasound-assisted in electrodeposition process can improve current distribution on cathode and accelerate mass transfer rate, which is beneficial to promote nucleation and refine grains size, thus improving the overall properties of coating. At present, most of the researches on ultrasound-assisted electrodeposition focus on cobalt or nickel binary alloy coatings [13-17]. Compared with binary alloy coatings, ternary alloy coatings have better mechanical property. Therefore, Ni-Co-Fe alloy coating was prepared on the surface of copper by ultrasound-assisted electrodeposition to greatly improve the mechanical property of copper.

2. EXPERIMENTAL

2.1 Materials

Wire cutting method is used to cut copper as substrate material with size of 50 mm×30 mm×2 mm. The substrate is polished, chemically oiled, pickled activated and cleaned with deionized water sequentially. And then, the substrate is dried in a drying oven. Table 1 shows the solution composition and technological conditions of oil removal and pickling activation.

Table 1. Solution composition and technological conditions of oil removal and pickling activation

Process	Solution composition	Technological conditions
Oil removal	NaOH 30 g/L, Na ₂ CO ₃ 15 g/L, Na ₃ PO ₄ 6 g/L	70°C, 6 min
Pickling activation	10% (volume fraction) hydrochloric acid	Room temperature, 1 min

2.2 Preparation of Ni-Co-Fe alloy coating

Ni-Co-Fe alloy coating was electrodeposited on the surface of copper substrate using the experimental device shown in Figure 1. The anode is electrolytic nickel plate and cathode is treated copper substrate. The anode area is twice as large as the cathode. Table 2 shows the main composition of the bath. The reagents used to prepare the bath are all analytically pure grade.

Ultrasound is generated by a constant frequency (40 kHz) ultrasound generator. When the ultrasound acts directly on the bath, special effects will be produced to affect the electrodeposition process of Ni-Co-Fe alloy coating. During the experiment, the bath temperature was maintained at about 50°C, while the current density and electrodeposition time was 3 A/dm² and 60 min, respectively under the condition of ultrasound power 0~240 W.

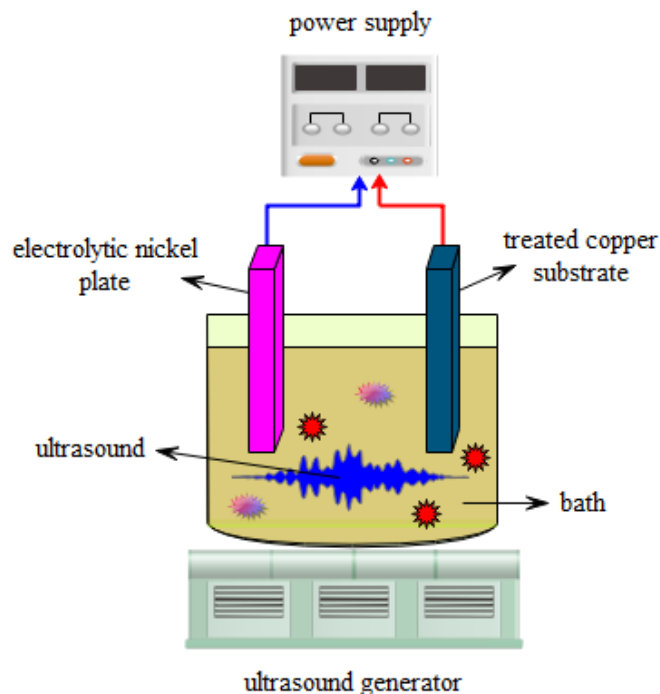


Figure 1. Schematic diagram of experimental device

Table 2. Main composition of the bath

Reagents	Concentration/ (g·L ⁻¹)
NiSO ₄	240
NiCl ₂	35
CoSO ₄	20
FeSO ₄	12
H ₃ BO ₃	50

2.3 Testing and analysis of Ni-Co-Fe alloy coating

After cleaning, the Ni-Co-Fe alloy coating sample was put into the oven at 200°C for 2 hour to remove hydrogen and eliminate stress. And then, it was cut for testing and analysis as required.

2.3.1 Surface morphology and microstructure

The surface morphology of copper and Ni-Co-Fe alloy coatings was observed by S-4800 scanning electron microscope respectively. The microstructure of Ni-Co-Fe alloy coatings was analyzed by electron diffraction (XRD) analysis using JEM-2010 high resolution transmission electron microscope. The grains size of Ni-Co-Fe alloy coatings was measured and the grains size distribution was plotted.

2.3.2 Hardness testing

The hardness of copper and Ni-Co-Fe alloy coatings was measured by 401-MVD Vickers hardness tester respectively. The applied load was 0.49 N, and the load was uniformly unloaded after 15 s. Five different positions on the sample surface were selected to measure, and the results were averaged to reduce errors. In addition, the surface hardness indentation of copper and Ni-Co-Fe alloy coatings was observed by scanning electron microscope.

2.3.3 Elastic modulus and elastic recovery property

The load-displacement curves of copper and Ni-Co-Fe alloy coatings were measured by Nanoindenter G200 nano-indentation instrument, and the load changes were automatically controlled by computer. The maximum load is 200 mN and the load retention time is 60 s. The elastic modulus was calculated by Oliver-Pharr method, and the elastic recovery property of copper and Ni-Co-Fe alloy coatings was evaluated by combining the maximum indentation depth and the recovery of indentation depth after unloading.

2.3.4 Friction and wear property

The friction coefficient of copper and Ni-Co-Fe alloy coatings was measured by XP-5 friction and wear tester at room temperature. The GCr15 steel ball was as the grinding piece, the load was 5 N and the friction time and length was 360 s and 6 mm, respectively. After the friction test, the abrasive debris on the sample surface was cleaned, and then the BSA2202S electronic balance was used to weigh the wear loss of copper and Ni-Co-Fe alloy coatings.

3. RESULTS AND DISCUSSION

3.1 Surface morphology and microstructure of different Ni-Co-Fe alloy coatings

Figure 2(a) shows the surface morphology of copper, and Figure 2(b)~2(e) show the surface morphology of different Ni-Co-Fe alloy coatings prepared on the surface of copper by ultrasound-assisted electrodeposition under different ultrasound power. The comparison results show that the Ni-Co-Fe alloy coating can be completely covered on the surface of copper with and without ultrasound. However, ultrasound power has a certain influence on the surface morphology of the alloy coating. As the ultrasound power increases to 120 W, the grains of the alloy coating are refined and the surface tends to be flat and compact.

The reasons can be attributed to three aspects [18-20]: (1) ultrasound directly acts on the bath to produce cavitation effect which can strengthen the mass transfer process and accelerate the electrodeposition rate. Properly increasing the ultrasound power can effectively promote nucleation and reduce the critical nucleation radius, thereby achieving grain refinement. (2) Ultrasound acts

directly on the bath also can produce a strong shock wave, which will break the coarse grains into fine grains, and achieve heterogeneous nucleation to further improve the nucleation rate. (3) The transmission of ultrasound in the bath increases the local temperature of the contact interface between the electrodeposition surface and the bath, which enhances the activation effect of the deposition surface. Properly increasing the ultrasound power makes more metal ions participate in the reaction, which improves the electrodeposition efficiency and also helps to improve the surface morphology of the alloy coating. However, as the ultrasound power continues to increase from 120 W to 240 W, the grains of the alloy coatings are coarsened, accompanied by a decrease in surface compactness. This is because too much higher ultrasound power will generate flocculation and shock waves, which break the equilibrium state of the electrodeposition reaction, resulting in a decrease in the electrodeposition efficiency and deterioration of surface morphology.

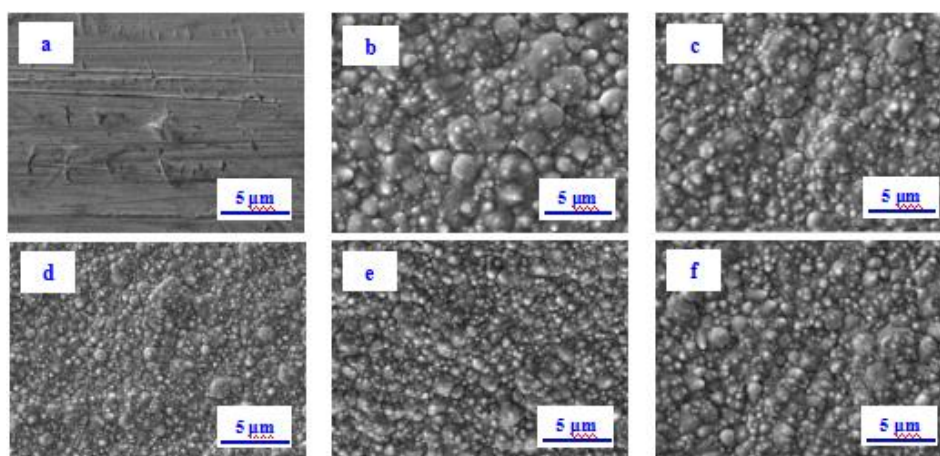


Figure 2. Surface morphology of copper and different Ni-Co-Fe alloy coatings: a-copper; b-Ni-Co-Fe alloy coating (ultrasound power 0 W); c-Ni-Co-Fe alloy coating (ultrasound power 60 W); d-Ni-Co-Fe alloy coating (ultrasound power 120 W); e-Ni-Co-Fe alloy coating (ultrasound power 180 W); f-Ni-Co-Fe alloy coating (ultrasound power 240 W)

In comparison, the Ni-Co-Fe alloy coating electrodeposited under ultrasound power 120 W has the best surface morphology. Figure 3 shows the electron diffraction pattern and grain size distribution of the Ni-Co-Fe alloy coating prepared under ultrasound power 120 W. As can be seen from Figure 3(a), the electron diffraction pattern shows many clear loop shapes similar to corrugation, indicating that the microstructure of the alloy coating is dense. It can be seen from Figure 3(b) that the grain size is concentrated in the range of 40~55 nm, indicating that the grain size of the alloy coating is relatively uniform. The average grain size is about 50 nm after selecting a certain number of grains, so it can be inferred that the Ni-Co-Fe alloy coating has nanocrystalline structure. The nanocrystalline structure of alloy coatings prepared by ultrasound-assisted electrodeposition has also been reported [21-23].

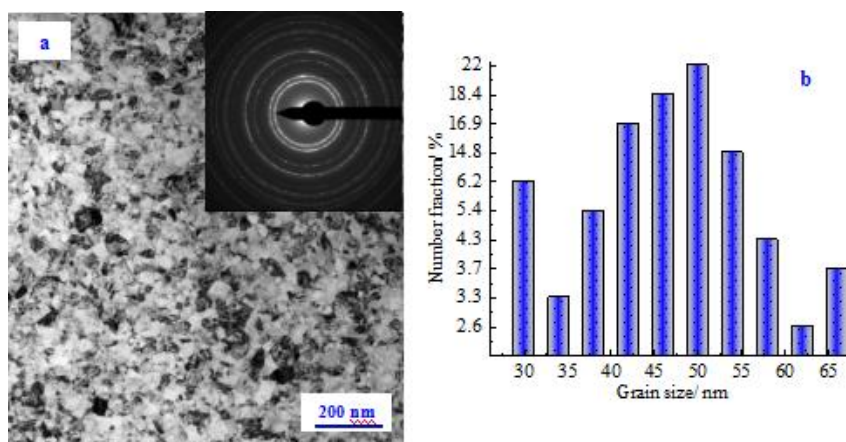


Figure 3. Electron diffraction pattern and grain size distribution diagram of the Ni-Co-Fe alloy coating electrodeposited under ultrasound power 120 W: a-electron diffraction pattern; b-grain size distribution diagram

3.2. Hardness and toughness of different Ni-Co-Fe alloy coatings

Figure 4 shows the hardness of different Ni-Co-Fe alloy coatings electrodeposited on the surface of copper under different ultrasound power. As can be seen from Figure 4, the hardness increases first and then decreases with the increase of ultrasound power. The reason is that the appropriate ultrasound power can promote crystallization nucleation and refine grain size leading to compact microstructure and enhancement of plastic deformation resistance. The ultrasonic on mechanical property of materials is studied in many papers. For example, Zheng studied the effect of ultrasonic power on mechanical property of Co-Cr₃C₂ coating [24]. Wang found that ultrasound is beneficial to improve the wear resistance of Ni-SiC composite coating [25]. However, when the ultrasound power is 120 W, the hardness of the as-prepared Ni-Co-Fe alloy coating reaches 652.6 HV, which is about 5 times higher than that of copper (106.8 HV). Due to the dense microstructure of the alloy coating, the plastic deformation degree is reduced when the hard indenter contacts the surface. However, too much higher ultrasound power leads to the deterioration of microstructure and decrease of plastic deformation resistance.

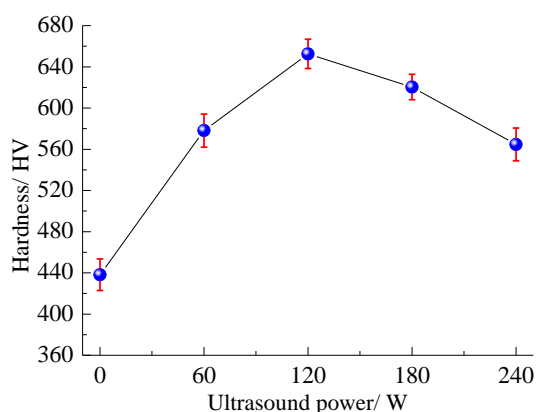


Figure 4. Hardness of different Ni-Co-Fe alloy coatings electrodeposited on the surface of copper under different ultrasound power

Figure 5 shows the hardness indentation on the surface of copper and the Ni-Co-Fe alloy coating electrodeposited under ultrasound power 120 W. It is observed that the surface hardness indentation of copper and Ni-Co-Fe alloy coating both shows regular diamond shape. However, the indentation size of the Ni-Co-Fe alloy coating is obviously smaller than that of the copper, which further confirms that Ni-Co-Fe alloy coating have strong resistance to plastic deformation resistance and high hardness. In addition, it is found that there are no obvious cracks on the indentation edges of the Ni-Co-Fe alloy coating, indicating that Ni-Co-Fe alloy coatings have good toughness.

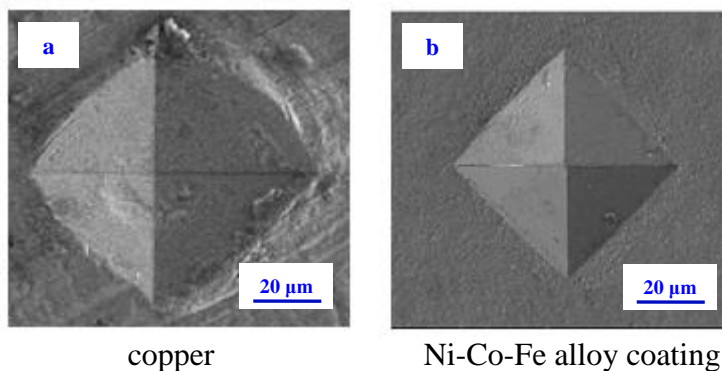


Figure 5. Hardness indentation on the surface of copper and the Ni-Co-Fe alloy coating electrodeposited under ultrasound power 120 W

3.3 Elastic modulus and elastic recovery property of different Ni-Co-Fe alloy coatings

Figure 6 shows the load-displacement curves of copper and different Ni-Co-Fe alloy coatings. It can be seen from Figure 6 that each curve is composed of a loading stage, a holding stage and an unloading stage.

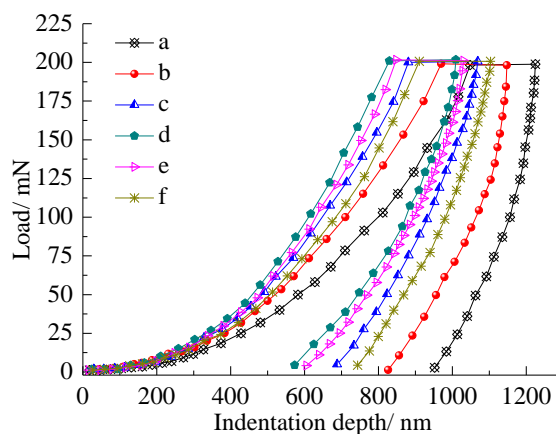


Figure 6. Load-displacement curves of copper and different Ni-Co-Fe alloy coatings: a-copper; b-Ni-Co-Fe alloy coating (ultrasound power 0 W); c-Ni-Co-Fe alloy coating (ultrasound power 60 W); d-Ni-Co-Fe alloy coating (ultrasound power 120 W); e-Ni-Co-Fe alloy coating (ultrasound power 180 W); f-Ni-Co-Fe alloy coating (ultrasound power 240 W)

The curves of each stage are relatively smooth, and there is no obvious sudden change, indicating that copper and different Ni-Co-Fe alloy coatings have uniform microstructure. In the loading stage, elastic deformation first occurs. As the load increases, the elastic deformation turns into plastic deformation to a certain extent. In the unloading stage, it is mainly the deformation recovery process, and the indentation is formed due to the large degree of plastic deformation.

The elastic modulus of copper and different Ni-Co-Fe alloy coatings is obtained according to the Oliver-Pharr equation, as shown in Figure 7. It can be seen from Figure 7 that as the ultrasound power increases, the elastic modulus increases first and then decreases. The analysis shows that the appropriate increase of ultrasound power can refine the grain size and enhance the plastic deformation resistance of the alloy coating, so that the elastic modulus increases. The relationship between grains size and mechanical property is reported in some papers [26-28]. However, too much higher ultrasound power leads to the deterioration of the surface morphology of the alloy coating and the weakening of the resistance to plastic deformation, so the elastic modulus decreases. The elastic modulus of the Ni-Co-Fe alloy coating electrodeposited under ultrasound power 120 W reaches 202.4 GPa, which is 1.8 times that of copper.

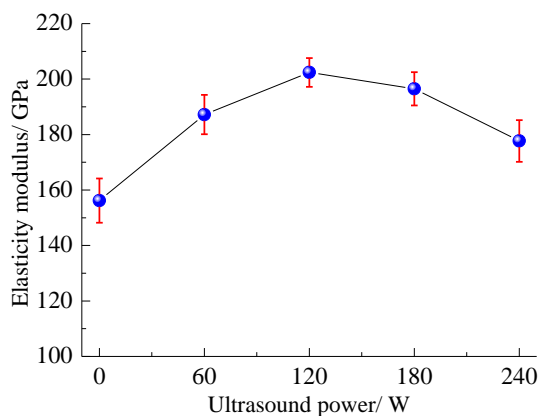


Figure 7. Elastic modulus of different Ni-Co-Fe alloy coatings electrodeposited on the surface of copper under different ultrasound power

The results show that the difference between the maximum depth of indentation during loading and unloading can reflect the elastic recovery ability of the coating. The elastic recovery ability of materials is investigated and reported in some literatures [29-31]. Figure 7 shows that the maximum indentation depth of copper is about 1224.6 nm, and the indentation depth after unloading is about 951.7 nm. Therefore, the recovery of indentation depth accounts for 22.3%. As the ultrasound power increases to 120 W, the proportion of indentation depth recovery of the alloy coating increases gradually, indicating that the elastic recovery ability is enhanced. However, as the ultrasound power increases from 120 W to 240 W, the proportion of indentation depth recovery decreases, indicating that the elastic recovery ability becomes worse. In comparison, the Ni-Co-Fe alloy coating electrodeposited under ultrasound power 120 W has the best elastic recovery ability, and the recovery of the indentation

depth accounts for about 40%, which is closely related to the dense microstructure and good resistance to deformation.

3.4 Friction and wear property of different Ni-Co-Fe alloy coatings

Figure 8 shows the friction coefficient and wear loss of different Ni-Co-Fe alloy coatings electrodeposited on the surface of copper under different ultrasound power. It can be seen from Figure 8 that with the increase of ultrasound power, the friction factor and wear loss both show a trend of first decreasing and then increasing. Appropriate ultrasound power makes the surface of the alloy coating tend to be flat and the microstructure tends to be dense, resulting in improvement of hardness and wear resistance. Many scholars have studied the effect of ultrasound on the wear resistance of materials [32-33]. The Ni-Co-Fe alloy coating electrodeposited under ultrasound power 120 W has the lowest friction coefficient (0.32) and wear loss (0.82 mg) which is approximate half of copper. Moreover, the Ni-Co-Fe alloy coating has compact surface with higher hardness and better resistance to plastic deformation, leading to the best wear resistance. However, too high higher ultrasound power leads to a decrease in the hardness of the alloy coating and plastic deformation resistance. During the friction process, the wear degree of the contact surface is increased, so the wear resistance is weakened, and both the friction coefficient and the wear loss increase.

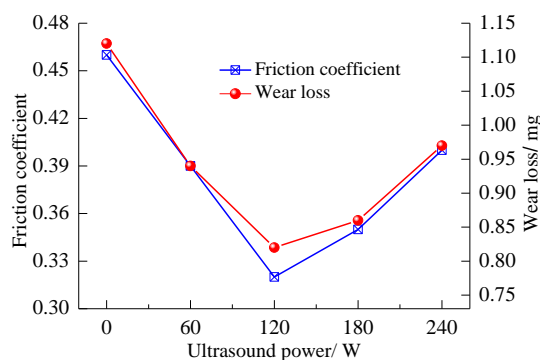


Figure 8. Friction coefficient and wear loss of different Ni-Co-Fe alloy coatings electrodeposited on the surface of copper under different ultrasound power

4. CONCLUSIONS

(1) During the electrodeposition of Ni-Co-Fe alloy coating, the applied ultrasound can strengthen mass transfer and refine the grains to obtain the Ni-Co-Fe alloy coating with compact surface and nanocrystalline structure. When the ultrasound power is 120 W, the hardness and elastic modulus of the as-prepared Ni-Co-Fe alloy coating increases, which is manifested as the enhancement of elastic recovery ability and wear resistance. However, too high higher ultrasound power has adverse effects, resulting in the deterioration of microstructure, the reduction of hardness, and the decline of both elastic recovery ability and wear resistance of Ni-Co-Fe alloy coating.

(2) The Ni-Co-Fe alloy coating electrodeposited under ultrasound power 120 W has dense microstructure and relatively uniform grains, with an average grains size of about 50 nm. Compared with copper, the hardness and elastic modulus of the alloy coating are increased by about 5 times and 0.8 times, respectively. The Ni-Co-Fe alloy coating electrodeposited under ultrasound power 120 W has the lowest friction coefficient and the smallest wear loss, showing good toughness and wear resistance which can significantly improve the mechanical property of copper.

ACKNOWLEDGEMENT

The study was supported by “Henan Education Department Project (20B140014)”.

References

1. L. H. Chan, K. Yasuda, J. M. Song and T. Suga, *Surf. Interface*, 28 (2022) 101620.
2. H. C. Aksa, I. Hacisalihoglu, F. Yildiz, T. Varol, O. Guler, G. Kaya and S. B. Akcay, *J. Mater. Process. Technol.*, 304 (2022) 117564.
3. Y. D. Yu, J. W. Lou, W. Li, L. X. Sun, H. L. Ge and G. Y. Wei, *Mater. Sci. Technol.*, 28 (2012) 448.
4. X. J. Li, M. Xu, J. H. Wang and H. Q. Xu, *J. Mater. Res. Technol.*, 15 (2021) 2345.
5. R. J. Ji, Y. H. Liu, S. To, H. Jin, W. S. Yip, Z. L. Yang, C. Zheng and B. P. Cai, *J. Alloys Compd.*, 764 (2018) 51.
6. A. Navaee and A. Salimi, *Appl. Surf. Sci.*, 440 (2018) 897.
7. P. W. Chou, J. M. Song, Z. Y. Xie, M. Akaike, T. Suga, M. Fujino and J. Y. Lin, *Appl. Surf. Sci.*, 456 (2018) 890.
8. A. Vanpariya, S. Khanna, P. Maratheey, S. Panaliya and I. Mukhopadhyay, *Mater. Today: Proc.*, 47 (2021) 691.
9. H. Firouzi-Nerbin, F. Nasirpouri and E. Moslehifard, *J. Alloys Compd.*, 822 (2020) 153712.
10. S. Z. Golkhatmi, M. Khalaj, A. Lzadpanahi and A. Sedghi, *Solid State Sci.*, 106 (2020) 106336.
11. Z. Yang, X. P. Liu and Y. L. Tian, *Colloids Surf., A*, 560 (2019) 205.
12. W. Xu, K. Rajan, X. G. Chen and D. K. Sarkar, *Surf. Coat. Technol.*, 364 (2019) 406.
13. C. Shen, X. D. Guan, Y. M. Tang, X. H. Zhao and Y. Zuo, *J. Electroanal. Chem.*, 902 (2021) 115793.
14. J. M. Costa and A. F. A. Neto, *Ultrason. Sonochem.*, 73 (2021) 105495.
15. I. Tudela, Y. Zhang, M. Pal, I. Kerr, T. J. Mason and A. J. Cobley, *Surf. Coat. Technol.*, 264 (2015) 49.
16. A. Li, Z. W. Zhu, Y. Liu and T. Y. Li, *Ultrason. Sonochem.*, 82 (2022) 105894.
17. Y. D. Yu, Z. L. Song, H. L. Ge and G. Y. Wei, *Prog. Nat. Sci.: Mater. Int.*, 24 (2014) 232.
18. L. Gong, F. J. Zhao, Z. Wang, Q. X. Sui, S. R. Xu, B. Liu, Q. Yuan, H. Wen, T. Y. Xiao, G. Liu, J. Liu and Z. H. Z. Chen, *Mater. Lett.*, 317 (2022) 132029.
19. A. Ahooei, S. Norouzi-Apourvari, A. Hemmati-Sarapardeh and M. Schaffie, *J. Pet. Sci. Technol.*, 195 (2020) 107734.
20. W. H. Zhou, J. Y. Tang, W. Shao and J. Wen, *Int. J. Mech. Sci.*, 222 (2022) 107248.
21. J. W. Bae, P. Asghari-Rad, A. Amanov and H. S. Kim, *Mater. Sci. Eng., A*, 826 (2021) 141966.
22. J. Oh, H. D. Park, M. Gwak, J. Lee, S. Son, A. Amanov, H. S. Kim, J. B. Seol, H. Sung and J. G. Kim, *Mater. Sci. Eng., A*, 812 (2021) 141101.
23. A. V. Panin, E. A. Melnikova, O. B. Perevalova, Y. I. Pochivalov, M. V. Leontyeva-Smirnova, V. M. Chernov and Y. F. Ivanov, *Phys. Mesomech.*, 12 (2009) 150.
24. X. H. Zheng, M. Wang, H. Song, D. Wu, X. T. Liu and J. Tan, *Surf. Coat. Technol.*, 325 (2017) 181.

25. H. Wang, H. J. Liu, Y. He, C. Y. Ma and L. Z. Li, *J. Mater. Eng. Perform.*, 30 (2021) 1535.
26. X. W. Fang, J. N. Yang, S. P. Wang, C. B. Wang, K. Huang, H. N. Li and B. H. Lu, *J. Mater. Process. Technol.*, 300 (2022) 117430.
27. A. Kalinenko, I. Vysotskii, S. Malopheyev, S. Mironov and R. Kaibyshev, *Mater. Sci. Eng., A*, 817 (2021) 141409.
28. S. Paul, U. Pal and S. K. Pradhan, *J. Alloys Compd.*, 858 (2021) 157732.
29. C. Q. Yan, L. X. Yuan, X. T. Yu, S. Z. Ji and Z. F. Zhou, *Constr. Build. Mater.*, 322 (2022) 125806.
30. X. L. Wang, Y. Su, S. Y. Han, M. A. Crimp, Y. P. Wang and Y. Wang, *Composites, Part B*, 216 (2021) 108832.
31. D. Q. Doan, T. H. Fang, A. S. Tran and T. H. Chen, *Comput. Mater. Sci.*, 170 (2019) 109162.
32. Y. J. Xue, W. Ma, J. S. Li and M. D. Duan, *Int. J. Surf. Sci. Eng.*, 4 (2010) 202.
33. C. S. Liu, X. Y. Huang, R. Xu, Y. J. Mai, L. Y. Zhang and X. H. Jie, *J. Mater. Eng. Perform.*, 30 (2021) 2514.

© 2022 The Authors. Published by ESG (www.electrochemsci.org). This article is an open access article distributed under the terms and conditions of the Creative Commons Attribution license (<http://creativecommons.org/licenses/by/4.0/>).